

# Blood Noise Reduction in Intravascular Ultrasound Imaging

Aage Gronningsaeter, Bjørn A. J. Angelsen, *Senior Member, IEEE*,  
Audun Gresli, Hans G. Torp, *Member, IEEE*, and David T. Linker

**Abstract**—Scattering from red blood cells (blood noise) increases significantly as the ultrasound frequency is increased above 10 MHz. This reduces the contrast between the vessel wall and the lumen in intravascular ultrasound imaging which makes it difficult to localize the vessel wall and plaque. A blood noise filter based on beam tilting and digital lateral low pass filtering is described. Beam tilting introduces a Doppler shift from blood which results in a frequency separation of the vessel wall signal and the blood noise. The performance of the filter is investigated by simulations and by *in vitro* experiments. The filter is found to be effective for blood velocities exceeding approximately 50 cm s<sup>-1</sup> at a 20 MHz ultrasound frequency with a beam tilt angle of 10 degrees and a frame rate of 15 f.p.s. By increasing the system frequency to 40 MHz, increase the beam tilt angle to 15 degrees and reduce the frame rate to 10 f.p.s., the filter is effective for blood velocities below 10 cm s<sup>-1</sup>.

## I. INTRODUCTION

**I**NTRAVASCULAR ultrasound imaging has developed rapidly since the end of the 1980s [1]–[7]. Interesting applications are lumen area measurements, plaque characterization and 3D lumen imaging. In order to achieve acceptable resolution with small catheters (<10 F), a high ultrasound frequency ( $f = 10\text{--}40$  MHz) is required. As the ultrasound frequency is increased above 10 MHz, scattering from blood (blood noise) becomes apparent, reducing the contrast between the lumen and the vessel wall. In real time imaging it may still be possible to see the transition between the blood and the vessel wall due to the temporal fluctuation of the blood noise [7]. However, on frozen images the blood noise makes it difficult to trace the vessel wall for measurements and 3D-reconstruction.

It is of great clinical value to obtain a precise definition of the border between blood and the vessel wall, for instance for device sizing and stent placement. Applying a blood noise filter would make the discrimination simpler in both real time imaging and on still images. However, soft plaque and stagnant blood represents a challenge since the acoustic impedance differ little from that of blood. The result is low scatter from the plaque which requires a very effective blood noise filter in order to differentiate it from blood.

Recently available fast analog to digital converters and random access memories make it possible to acquire and store the received high frequency ultrasound RF-signal in real time. This means that digital signal processing algorithms can be applied to the linear RF-signal along the beam (radial direction), from pulse to pulse (lateral direction) and from frame to frame (along the image frame coordinate or temporal direction). This opens up for noise reduction techniques that were not possible with analog techniques, however little work is published in this field so far. Some papers describe common imaging artifacts and geometric errors in intravascular ultrasound imaging without specifying signal processing that may correct for it [8]–[12].

The linear RF-signal contains information about scattering properties and movements of the biological structures. The sampling interval along the beam is in the order of 0.1  $\mu$ s, so short that movements in tissue or blood can hardly be registered from sample to sample. However, it is possible to observe changes in the vessel wall and blood signal in the lateral direction and along the image frame coordinate since the sampling intervals are in the order of 1 ms and 100 ms, respectively.

This paper presents one method for blood noise reduction based on signal processing in the lateral direction. The blood movement makes it possible to discriminate the blood signal from the vessel wall signal. The lateral power spectrum from a fixed vessel wall will be centered around zero frequency, and the shape of the spectrum is primarily determined by the beam profile. The lateral (temporal) frequency content is inversely proportional to the transit time which is given by the beam profile and the beam angular velocity. Blood that is not moving yields a spectrum of the same shape and frequency content. However, as the blood velocity increases, the transit time drops and the spectrum broadens.

If the ultrasound beam is tilted a few degrees up or down stream, then a Doppler shift is introduced in the blood noise, and a frequency separation between vessel wall signal and blood noise occur. A lateral low pass filter implemented in each depth location will pass the vessel wall signal through while fractions of the blood noise is suppressed.

Blood noise is primarily caused by scattering from the red blood cells. These are disc shaped and approximately 2  $\mu$ m thick and 7  $\mu$ m in diameter. The scattering intensity from blood is frequency dependent. Shung et al. [13] has reported a frequency dependency equal to  $f^4$  (Rayleigh scattering) for frequencies up to approximately 15 MHz, and Lockwood et al. [14] has measured it to approximately  $f^{1.35}$  in the 35–65 MHz

Manuscript received February 23, 1994; revised June 3, 1994.

A. Gronningsaeter, B. A. J. Angelsen, and H. Torp are with the Department of Biomedical Engineering, University of Trondheim, Medical Technical Center, 7005 Trondheim, Norway.

A. Gresli is with AUROTECH Electronics AS, N-7590 Tydal, Norway.

D. T. Linker is with the Division of Cardiology RG-22, University of Washington, Seattle, WA 98195 USA.

IEEE Log Number 9407883.

TABLE I  
SYMBOLS AND ABBREVIATIONS

$r$	Range, radial/axial coordinate
$r_o$	One particular observation depth
$\phi$	Beam angle, lateral coordinate
$\psi$	Beam tilt angle, azimuthal coordinate
$a$	Transducer radius
$c$	Velocity of sound
$f_m$	Frame rate
$A(\phi, \psi)$	Transducer angular sensitivity function (two-way)
$\sigma(r, \phi, \psi)$	Spatial scattering distribution
$g(r, \phi, \psi)$	Received ultrasound RF-signal
$f_o$	Center frequency of transmitted pulse
$f_d$	Doppler shift
$k_o$	Wave number (at transmit pulse center frequency)
$k_r, k_\phi, k_\psi$	Radial, lateral and azimuthal spatial frequency
$P_{g\phi}(k_\phi)$	Power spectrum in the lateral direction (constant depth)
$k_{s\phi}$	Lateral spatial sampling frequency
$f_{s\phi}$	Lateral temporal sampling frequency
$f_\phi$	Lateral temporal frequency
$V_B$	Blood velocity in the X1-direction
$V_{vw}$	Vessel wall velocity in the X2X3-plane
$V_{CT}$	Catheter tip velocity in the X2X3-plane (catheter whip)
$k_{BSB}$	Blood spectrum broadening factor
<b>QD</b>	<b>Quadrature Demodulated</b>
<b>ESR</b>	<b>Echo Signal Response</b>
<b>BNRR</b>	<b>Blood Noise Reduction Ratio</b>

frequency range. The blood scatter will increase significantly as the ultrasound frequency is increased above 10 MHz as illustrated in Fig. 1 where three images at 10, 20 and 30 MHz are compared (all acquired under different conditions).

In Section II.A, a linear model for the received RF-signal is presented, valid close to the focus of the beam. This model is used to derive an expression for the power spectrum in the lateral direction. Section II.B lists some typical blood, vessel wall and catheter tip velocities and their frequency shift and broadening effects on the power spectrum in the lateral direction. Section II.C presents a simulation that quantifies possible frequency separation and blood noise reduction in case an ideal lateral low pass filter is applied. Section III demonstrates blood noise reduction by an in vitro experiment with a simple lateral FIR-filter applied. Data is acquired from a rubber hose flushed with a blood mimicking liquid.

The symbols and abbreviations that occur most frequently in the paper are listed in Table I.

## II. SIGNAL ANALYSIS

### A. Signal Model

The ultrasound spatial RF image is formed by assigning the received RF-signal from a defined beam direction, to the image along the direction of the beam-axis, using the time to range transform:  $r = ct/2$ . The angular coordinates of the image are

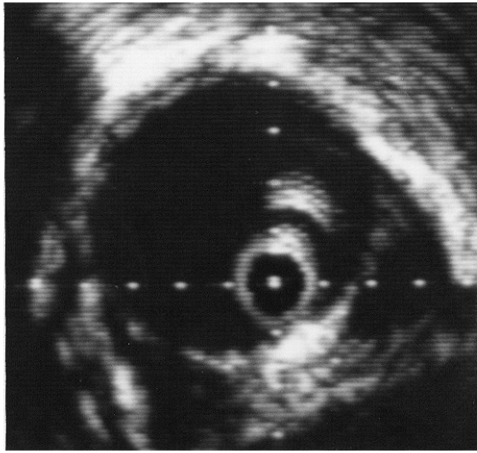
the same as the angular coordinates of the beam axis. The total received RF-signal is the superposition of the contribution of the individual scatterers, hence the complex pre-envelope can be written as an integral:

$$g(r, \phi, \psi; r', \phi', \psi') = \int dr' r'^2 d\phi' d\psi' \text{ESR}(r, \phi, \psi; r', \phi', \psi') \sigma(r', \phi', \psi') \quad (1)$$

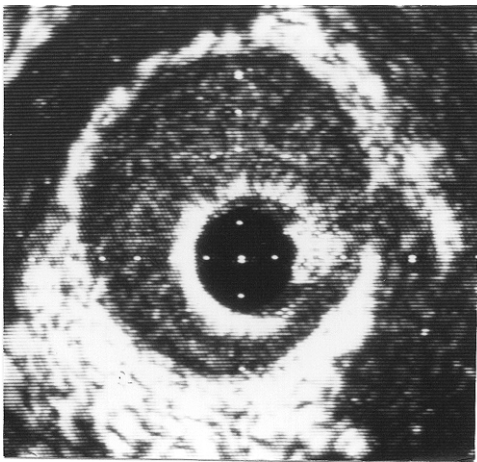
where the scatterer coordinates are  $(r', \phi', \psi')$  and the image coordinates are  $(r, \phi, \psi)$  as shown in Fig. 2. The expression  $dr' r'^2 d\phi' d\psi'$  is a small volume element in the scatterer space.

The spatial scattering distribution is denoted  $\sigma(r', \phi', \psi')$  and the echo signal response  $\text{ESR}(r, \phi, \psi; r', \phi', \psi')$  is the signal from a point scatterer located at  $(r', \phi', \psi')$ . The angular variation of the ESR is determined by the beam profile, and the range variation is determined by the received pulse. The received pulse waveform depend in general on the location of the scatterer within the beam, but close to the focus one can separate the range and angular dependency. The echo signal response (complex pre-envelope) can then be written

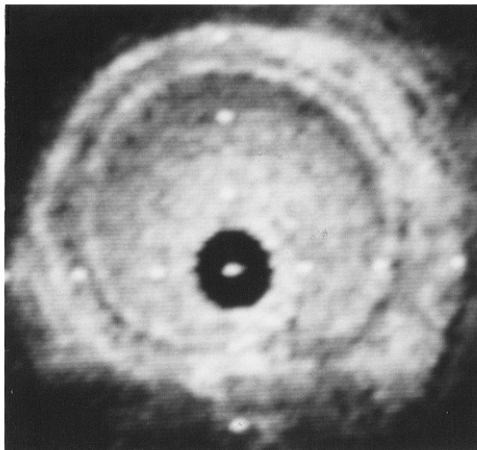
$$\text{ESR}(r, \phi, \psi; r', \phi', \psi') = \alpha(r, r') \frac{1}{r'^2} u \left[ \frac{2}{c} (r - r') \right] \times e^{i2k_o(r-r')} A(\phi - \phi', \psi - \psi') \quad (2)$$



(a)



(b)



(c)

Fig. 1. (a) 10 MHz image of pig ascending aorta. Blood noise is not visible. (Rotating mirror catheter, CVIS); (b) 20 MHz image of pig ascending aorta. Blood noise is visible. (Rotating mirror catheter, CVIS); (c) 30 MHz image of human external iliac. Blood noise represents a major contrast problem. (Rotating transducer catheter, Boston Scientific)

$\alpha(r, r')$  is a gain factor including the amplitude of the transmitter, the insertion loss of the transducer, the range dependent

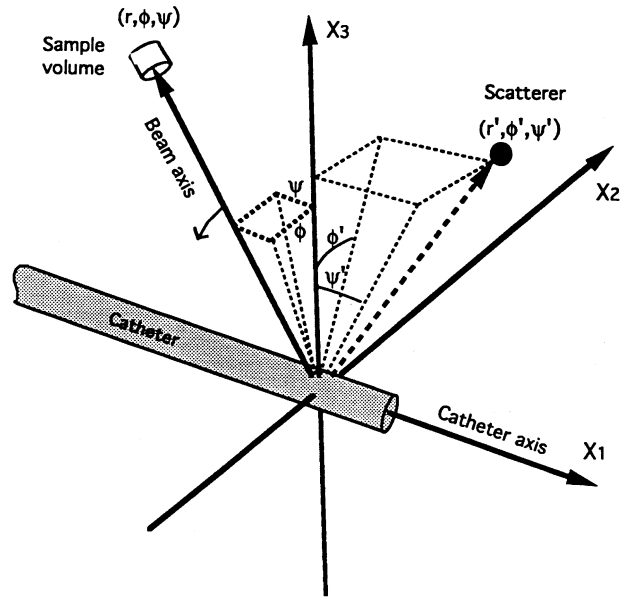


Fig. 2. Coordinate system for intravascular ultrasound imaging with a catheter. The beam coordinates are given by  $(r, \phi, \psi)$  and the scatterer or object coordinates are specified by  $(r', \phi', \psi')$ .

receiver gain (time gain compensation, TGC) and frequency dependency of the scattering and absorption in the medium.

$r'^{-2}$  takes care of loss due to spherical wave expansion by diffraction in the transmit and receive beams.

$u(\cdot)$  is the complex envelope of the signal received from a point scatterer.

$k_0$  is the wave number,  $k_0 = \omega_0/c = 2\pi f_0/c$

$e^{i2k_0(\cdot)}$  describes the complex phase of the signal.

$A(\cdot)$  is the two way angular sensitivity function of the transducer.

Equation (2) is spatially invariant in  $\phi$  and  $\psi$ , but not in range due to the spherical wave expansion  $1/r'^2$  and the gain factor  $\alpha(r, r')$ . The gain factor can be approximated by a constant by proper time gain compensation and by neglecting frequency dependent scattering and attenuation. The received RF-signal can then be written

$$g(r, \phi, \psi) = \alpha \int dr' d\phi' d\psi' u \left[ \frac{2}{c}(r - r') \right] e^{i2k_0(r-r')} \times A(\phi - \phi', \psi - \psi') \sigma(r', \phi', \psi') \quad (3a)$$

$$g(r, \phi, \psi) = \alpha \int dr' d\phi' d\psi' \times h(r - r', \phi - \phi', \psi - \psi') \sigma(r', \phi', \psi') \quad (3b)$$

which is a convolution between the spatial scattering distribution and a spatial invariant impulse response  $h(r, \phi, \psi)$  define by

$$h(r, \phi, \psi) = u \left[ \frac{2r}{c} \right] e^{i2k_0 r} A(\phi, \psi). \quad (4)$$

This model will be used to derive an expression for the power spectrum in the lateral direction.

*Doppler Shift:* Scatterer movement along the beam axis will generate a Doppler shift in the received signal. This can be seen from the complex envelope of the echo response from

a single scatterer which is obtained by multiplying the echo signal response in (2) with  $e^{-i2k_0r}$  (quadrature demodulation):

$$\begin{aligned} \text{ESR}_{\text{QD}}(r, \phi, \psi; r', \phi', \psi') &= \alpha(r, r') \frac{1}{r'^2} u \left[ \frac{2}{c} (r - r') \right] \\ &\times e^{-i2k_0r'} A(\phi - \phi', \psi - \psi') \end{aligned} \quad (5)$$

This equation describes a complex low pass signal in both the radial and the lateral direction. The radial position versus time for a point scatterer that moves with velocity  $v_r$  along the beam axis is

$$r' = r'_0 + v_r t \quad (6)$$

where  $r'_0$  is the range at  $t = 0$ . Inserting this equation into the complex phase term of (5) yields

$$e^{-i2k_0r'} = e^{-i2k_0r'_0} e^{i2\pi f_d t}. \quad (7)$$

The first phase factor depends on the scatterer position at  $t = 0$  while the second term relates complex phase and scatterer velocity through the Doppler equation:

$$f_d = -2 \frac{f_0}{c} v_r \quad (8)$$

*Power Spectrum in the Lateral Direction:* The ultrasound beam scans 360 degrees around the catheter axis, sending repetitive pulses, uniformly spaced in angle. The two dimensional (2D) image presented on the screen is a 2D mapping of a 3D scattering distribution. When the signal is analyzed in one dimension only (in the radial, lateral or temporal direction), then a 3D scattering distribution is mapped to a 1D signal. A model for the 1D lateral power spectrum from stationary scatterers is found, making the following assumptions: The scatterers are small compared to the wavelength and randomly distributed, i.e. the spatial power spectral density from the scatterers is constant. Then the Wiener-Khintchine theorem [15] can be applied to the Fourier transform of (3) and integration over the elevation frequency range  $k_\psi$  can be performed. By setting the range parameter constant, the following expression is obtained, see Appendix:

$$P_{g\phi}(k_\phi) \sim \int dk_\psi |A_{\text{FT}}(k_\phi, k_\psi)|^2 \quad (9)$$

where  $A_{\text{FT}}(k_\phi, k_\psi)$  is the two dimensional spatial Fourier transform of the two way angular sensitivity function  $A(\phi, \psi)$ .

A specific solution to (9) is required for quantitative assessments on blood noise reduction by lateral filtering. The simple analytical expression for the far field radiation from a plane circular piston transducer (excited uniformly by continuous

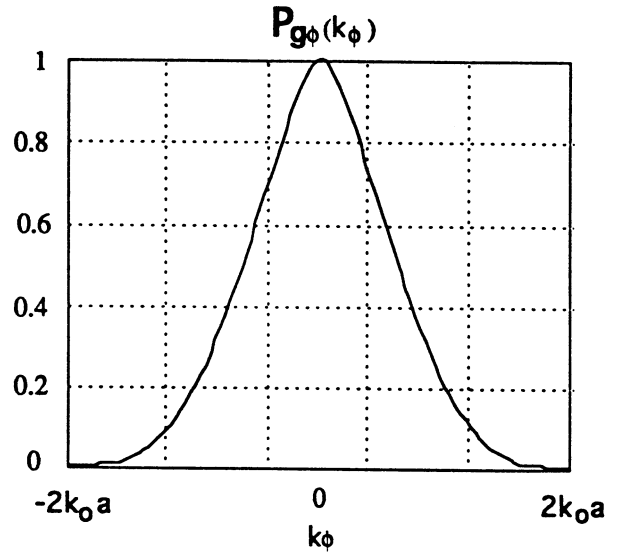


Fig. 3. Model for the power spectrum in the lateral direction from a large number of small, randomly distributed and stationary scatterers. The spatial frequency content is limited to  $\pm 2k_0a$ , where “ $a$ ” is the transducer radius and “ $k_0$ ” is the wave number.

waves) has been used to derive the following expression [16] as shown in (10) at the bottom of this page. Equation (10) describes a circular symmetric cone shaped function. The model of the lateral power spectrum  $P_{g\phi}(k_\phi)$  is now found by numerical integration of (9) with (10) inserted. A linear plot is shown in Fig. 3. Note that this spatial frequency content from stationary scatterers is limited to

$$k_{\phi\text{Max}} = \pm 2k_0a. \quad (11)$$

The proposed model for the lateral power spectrum is only valid in the far field and for continuous wave excitation. Pulsed wave excitation changes the angular properties of the beam, but the error in lateral power spectrum is assumed to be low for relatively long transmit pulses like the ones that have been used in this work (transducer  $-6$  dB fractional bandwidth is  $\approx 25\%$ ).

The beam profile from a plane transducer expands proportional to range (in the far field). However, most intravascular catheters use a focused beam, either by curving the transducer or the mirror. In this case the beam expands more rapidly distal to the focus. The expression in (9)–(11) is only valid close to the focus. Distal to the focus, this model overestimates the lateral bandwidth.

*Sampling Criteria:* Three sampling criteria should be met in order to avoid aliasing:

$$\begin{aligned} A_{\text{FT}}(k_\phi, k_\psi) &= \begin{cases} \frac{4\pi^2\rho}{k_0^4} \left\{ 2k_0^2a^2 \cos^{-1} \left( \frac{k_t}{2k_0a} \right) - k_t k_0 a \sqrt{1 - \left( \frac{k_t}{2k_0a} \right)^2} \right\} & k_t < 2k_0a \\ 0 & \text{elsewhere} \end{cases} \\ k_t &= \sqrt{k_\phi^2 + k_\psi^2} \end{aligned} \quad (10)$$

- a) In the radial direction, a sampling frequency of at least twice the bandwidth of the transducer is required (typical values: 10–40 MHz).
- b) In the lateral direction, the beam density should ensure sufficiently beam overlap in order to avoid aliasing in the lateral *spatial* frequency domain. The lateral spatial sampling frequency  $k_{s\phi}$  equals the number of beams per revolution  $N_b$ , and this number should be no less than twice the maximum spatial frequency component from stationary tissue (see (11)):

$$N_b \geq 4k_0 a \quad (12)$$

Typical value:  $N_b \geq 225$  ( $a = 0.7$  mm,  $f_0 = 20$  MHz,  $c = 1560$  m s<sup>-1</sup>).

- c) The lateral *temporal* frequency is proportional to the lateral *spatial* frequency, the constant of proportionality is  $f_m$ , the frame rate, see (13a). The *spatial* frequency (unit less) in a specific depth is independent on the speed of rotation, while the *temporal* frequency (in Hz) equals the product of the frame rate and the spatial frequency. The lateral temporal *sampling* frequency is given by (13b)

$$f_\phi = f_m k_\phi \quad (13a)$$

$$f_{s\phi} = f_m k_{s\phi} = f_m N_b \quad (13b)$$

and  $f_{s\phi}$  should be no less than twice the maximum temporal frequency component from the Doppler shifted and broadened spectrum from blood which typically ranges between 5–15 kHz. Lateral temporal sampling frequencies in the range 10–30 kHz is therefor required. The corresponding beam densities are  $N_b = 666$ –2000 at the typical frame rate  $f_m = 15$  f.p.s.

### B. Signal Properties in the Lateral Direction

**Doppler Shifts:** Three kind of movements cause radial velocity components along the beam axis as illustrated in Fig. 4: blood flow in the  $X_1$ -direction (if the beam is tilted), vessel wall and catheter tip velocities.

The corresponding Doppler shifts are given by

$$f_{d,\text{Blood}} = -2 \frac{f_0}{c} V_B \sin(\psi) \quad (14)$$

$$f_{d,\text{VW}} = -2 \frac{f_0}{c} V_{\text{VW}} \cos(\psi) \quad (15)$$

$$f_{d,\text{CT}} = -2 \frac{f_0}{c} V_{\text{CT}} \cos(\psi). \quad (16)$$

The Doppler shift from blood increases with the beam tilt angle at the expense of geometrical distortion of the displayed image. This distortion equals  $1/\cos(\psi)$  unless it is compensated for (1.5% error for  $\psi = 10^\circ$ ). A minor drop in back scattered intensity is expected due to beam tilting in the range 5–15 degrees [17], [18]. The Doppler shifts in (14)–(16) may be directed in the same or in the opposite direction along the frequency axis depending on: the beam tilt angle, the direction of blood flow relative the catheter tip, catheter tip movement and whether the blood flow is systolic (peripheral arteries) or diastolic (coronary arteries). A description of some typical blood, vessel wall, and catheter tip velocities is listed below in order to quantify the Doppler shifts.

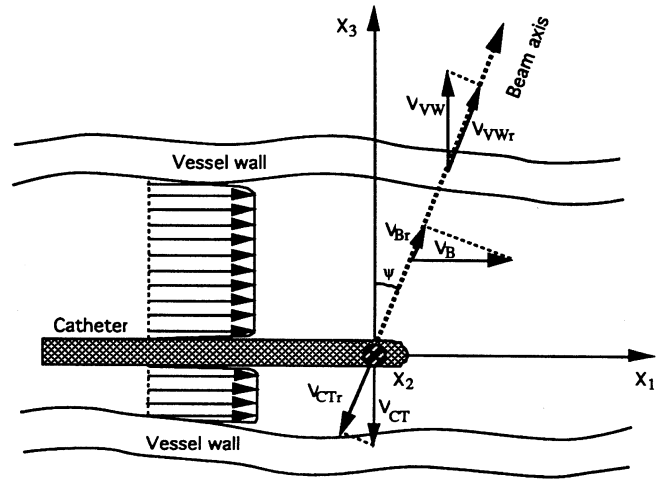


Fig. 4 Three kinds of movement yield velocity components in the radial beam direction: \* Blood flow with velocity  $V_B$  in the catheter axial direction. \* Vessel wall dilatation of velocity  $V_{\text{VW}}$ . \* Catheter tip translation with velocity  $V_{\text{CT}}$  perpendicular to the catheter axis. The components of these velocities in the beam radial direction are  $V_{\text{Br}}$ ,  $V_{\text{VWr}}$  and  $V_{\text{CTr}}$ , respectively.

**Blood Velocities:** The *phasic* blood velocity is highest in the ascending aorta, with typical systolic peak velocity being 100 cm s<sup>-1</sup> [19]. The peak velocity will be lower in the peripheral and coronary arteries. Typical peak velocities in the femoral and the iliac artery are 40–80 cm s<sup>-1</sup> [19], [20], with systolic flow dominating. In the coronary arteries, diastolic flow dominates, and peak velocities exceeding 50 cm s<sup>-1</sup> may occur [21], [22]. However, there are large variations in what is normal.

**Vessel Wall Velocities:** Published work on measurements of vessel wall velocities is sparse. One paper describes the measurement of the diameter of a femoral artery with an A-mode ultrasound instrument by tracking the two vessel walls with two independent phase locked loop systems [23]. The following maximum vessel wall velocity was calculated from the diameter traces:  $V_{\text{VW}} \approx 2.7$  mm s<sup>-1</sup>.

More data is available on radial dilatation: the relative change in vessel radius  $\Delta r/r$ . Nichols tabulates some measured values for some peripheral and coronary arteries in humans and dogs [19]. Values exceeding 5% rarely occur. Assume that the maximum vessel wall velocity occurs during the rise time of the systolic pressure, here estimated to last a minimum of  $\Delta T_{\text{min}} = 100$  ms, then the maximum radial vessel wall velocity can be estimated to:  $V_{\text{VWmax}} \approx \Delta r_{\text{max}}/\Delta T_{\text{min}} = 0.25 D$  [ mm s<sup>-1</sup>] where  $D$  is the diameter of the vessel (in mm). Applied to arteries of diameter 3 mm and 10 mm, the estimated maximum vessel wall velocities are 0.75 mm s<sup>-1</sup> and 2.5 mm s<sup>-1</sup>, respectively.

**Catheter Tip Velocities:** The catheter tip velocity adds to the vessel wall velocity, i.e. the measured Doppler shift is caused by the relative velocity between the catheter tip and the vessel wall. In contrast to vessel wall velocities that are often directed in the radial direction (with reference to Fig. 2), the catheter tip movement will often follow a back and forth translation in the  $X_2/X_3$  plane. The result is a Doppler shift that depends on the beam lateral scan position. The Doppler shift may for example be at its maximum when the beam is

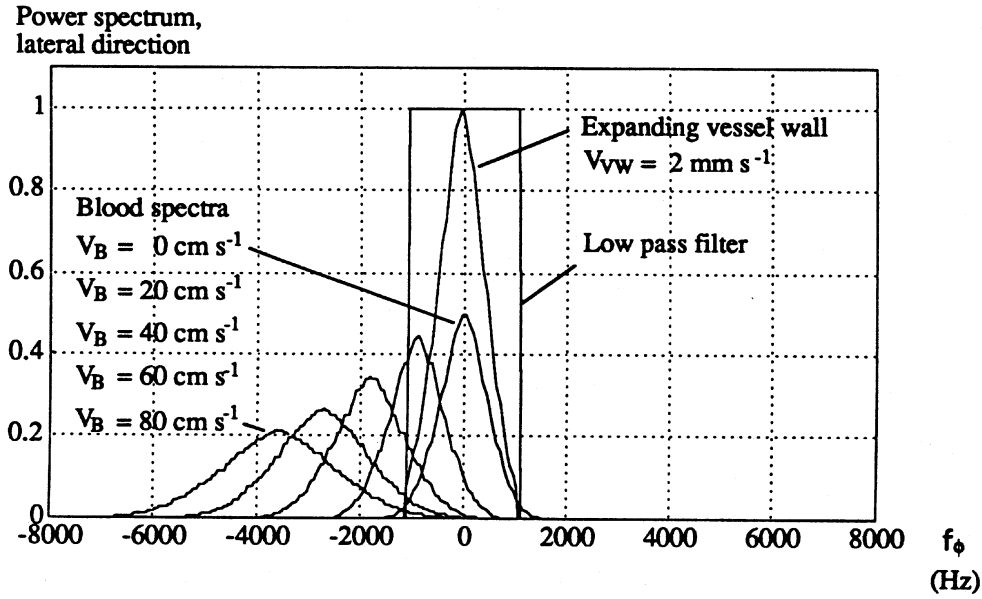


Fig. 5. Simulated temporal power spectrum in the lateral direction from an expanding vessel wall and from blood in a typical 20 MHz imaging situation. The lateral filter used for blood noise reduction is an ideal low pass filter with bandwidth equal to 65% of the bandwidth from stationary tissue.

directed in the 12 and 6 o'clock position, and zero in the 3 and 9 o'clock position.

*Spectrum Broadening:* The power spectrum from blood is subject to a frequency broadening due to reduced transit time through the sample volume as the blood velocity increases. Frequency broadening and Doppler shift can be described separately since the echo signal response (see (2)) is separable in range and angle. First consider no beam tilting: The transit time for scatterers that do not move relative to the catheter is determined by the beam profile and the velocity of the sample volume:  $V_{SV\phi} = 2\pi f_m r_0$  (the beam angular velocity times the observation depth  $r_0$ ). The scatterers traverse through the sample volume in a pure lateral direction (constant range). Blood flow in the  $X_1$ -direction introduces an azimuthal and a radial velocity component in addition. The sum of the lateral and the azimuthal components yields an angular velocity component (constant range) which determines the transit time. The spectrum from flowing blood will therefore be a broadened version of the spectrum from stationary scatterers when the beam is circular symmetric as stated in the model. A scale factor (equal to the ratio of the transit times for stationary and moving blood scatterers, respectively) is denoted the Blood Spectrum Broadening factor and given by

$$k_{BSB} = \sqrt{1 + \left(\frac{V_B}{V_{SV\phi}}\right)^2} = \sqrt{1 + \left(\frac{V_B}{2\pi f_m r_0}\right)^2} \geq 1. \quad (17)$$

The radial component generates one positive chirp as the scatterer enters the beam and one negative chirp as it leaves the beam. The result is frequency broadening, but simulations has shown that this effect is negligible.

Next consider beam tilting: Tilting the beam causes the broadened spectrum from flowing blood to be shifted in

frequency due to the radial velocity component (see (14)). The Doppler shift is sensitive to beam tilting while the transit time is not. Practical beam tilting causes no additional frequency broadening since the trajectory distance through the sample volume changes little by tilting the beam.

### C. Reduction of Blood Noise by Lateral Low Pass Filtering

A simulation is performed to demonstrate typical frequency separation by beam tilting and blood noise reduction by lateral low pass filtering:

*Frequency Separation:* First the lateral spectrum from an expanding vessel wall is found by using (9) (Fig. 3), convert it from spatial to temporal frequency by multiplying by  $f_m$  (see (13a)) and shift it according to the Doppler equation (15). Next, the spectrum from blood is calculated for several blood velocities and plotted in the same diagram for comparison. The same procedure is used for the blood spectrum except that (9) is first scaled in frequency and amplitude by  $k_{BSB}$  and  $1/k_{BSB}$ , respectively (see (17)). The result for a typical 20 MHz 8 F catheter is shown in Fig. 5 ( $V_{vw} = 2 \text{ mm s}^{-1}$ ,  $f_0 = 20 \text{ MHz}$ ,  $a = 0.7 \text{ mm}$ ,  $f_m = 15 \text{ f.p.s.}$ ,  $\psi = 10^\circ$ ,  $c = 1560 \text{ m s}^{-1}$  and  $r_0 = 3 \text{ mm}$ ).

The Doppler shift from the vessel wall is 50 Hz in this example, i.e. small compared to the bandwidth of the signal. Catheter tip movements will generate an additional Doppler shift in some beam directions. However, vessel wall and catheter tip velocities in the order of  $1 \text{ mm s}^{-1}$  generate so small Doppler shifts that the effect can be neglected in the design of the lateral low pass filter.

*Lateral Filtering:* An ideal low pass filter is used in the simulation to quantify potential blood noise reduction by lateral filtering. The filter frequency response is centered around zero frequency and should be broad enough to pass the vessel wall signal through with an acceptable level of distortion, the Doppler shift taken into account (negligible).

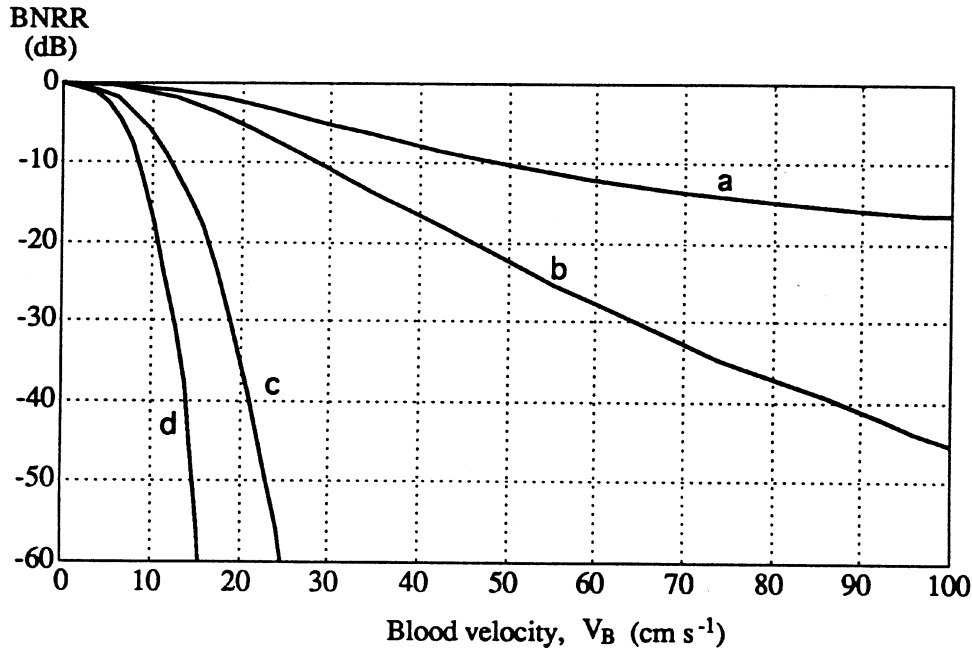


Fig. 6. Simulated Blood Noise Rejection Ratio (BNRR) versus the blood velocity for different scanning parameters ( $c = 1560 \text{ m s}^{-1}$  and  $r_0 = 3 \text{ mm}$ ): (a)  $f_0 = 20 \text{ MHz}$ ,  $a = 0.7 \text{ mm}$ ,  $f_m = 15 \text{ f.p.s.}$ ,  $\psi = 10^\circ$  (b)  $f_0 = 30 \text{ MHz}$ ,  $a = 0.4 \text{ mm}$ ,  $f_m = 15 \text{ f.p.s.}$ ,  $\psi = 10^\circ$  (c)  $f_0 = 30 \text{ MHz}$ ,  $a = 0.46 \text{ mm}$ ,  $f_m = 10 \text{ f.p.s.}$ ,  $\psi = 15^\circ$  (d)  $f_0 = 40 \text{ MHz}$ ,  $a = 0.35 \text{ mm}$ ,  $f_m = 10 \text{ f.p.s.}$ ,  $\psi = 15^\circ$ .

Fig. 5 illustrates that better blood noise reduction can be achieved by reducing the bandwidth of the filter. The side effect is reduced lateral resolution. The filter bandwidth was set to 65% of the total bandwidth from *stationary* tissue (see (11)) in the simulation, yielding a 1.7% (0.075 dB) drop in vessel wall signal power. This frequency narrowing is probably not far from what can be tolerated in a practical situation.

Now the Blood Noise Rejection Ratio is defined as the ratio of the noise power from flowing blood to the noise power from stationary blood:

$$\text{BNRR} = 10 \log \frac{P_{\text{blood } V_B \neq 0}}{P_{\text{blood } V_B = 0}} \quad (18)$$

This ratio is plotted in Fig. 6 for four different conditions: Curve (a) and (b) represent typical imaging situations with a 20 MHz 8 F and a 30 MHz 5 F catheter, respectively (same beam opening angle). The beam tilt angle is  $10^\circ$  and the frame rate is 15 f.p.s. In (c) and (d) the beam tilt angle is increased to  $15^\circ$  and the frame rate decreased to 10 f.p.s. in order to optimize for blood noise reduction at 30 and 40 MHz, respectively (at the expense of higher geometric distortion and a relatively low frame rate). This simulation demonstrates that the blood noise filter is effective ( $\text{BNRR} < -10 \text{ dB}$ ) for blood velocities exceeding  $\approx 50 \text{ cm s}^{-1}$  in a typical 20 MHz setup, but significant improvements can be made by optimizing for blood noise reduction.

### III. EXPERIMENTS

#### A. Materials and Methods

The work was carried out by doing computer simulations on a Macintosh computer and by in-vitro experiments in a vascular flow model. The RF-data was acquired with an intravascular scanner modified to collect sequences of full-

image, RF-data (CVIS Insight, Cardiovascular Imaging Systems, Inc., CA). Up to 14 frames were stored in memory and transferred to the computer for analysis and post processing.

The scanner was modified by including a quadrature demodulator at 20 MHz (mixing the band pass signal with two 20 MHz clocks, 90 degrees out of phase, followed by low pass filters). The in-phase and quadrature components were then digitized by the two already built in 8 bits AD-converters (20 M samples  $\text{s}^{-1}$ ). An analog logarithmic amplifier was used in the system in order to get a high dynamic range (approximately 55 dB). The disadvantage of nonlinear signal processing was assumed to be less than the advantage of a high dynamic range. Recently available AD-converters can digitize the band pass signal directly with 10 bits at 60 M samples  $\text{s}^{-1}$ , making both the log-amp and the analog quadrature demodulator obsolete in future designs.

The following setup was used for in vitro assessment of the blood noise filter: A 20 MHz, 8 F catheter with a rotating focused mirror (CVIS, Inc.) was located in a 45 cm long rubber hose of inner diameter 5 mm, the catheter tip was centered in the tube. The transducer radius was measured to  $a = 0.75 \text{ mm}$ , and the beam tilt angle was approximately 8 degrees. The focal depth was approximately 3.8 mm. Water containing blood mimicking particles (Sephadex G-25/Superfine, Pharmacia Fine Chemicals, Uppsala, Sweden) was flushed through the hose with a pump. The mean flushing velocity was adjustable and the velocity was calibrated by collected flow measurements. The data format was  $N_r = 64$  samples per beam,  $N_b = 1024$  beams per revolution, and the data was acquired with frame rate:  $f_m = 15 \text{ f.p.s.}$  The raw RF-data was transferred to a computer for lateral low pass filtering, decimation, magnitude detection, scan conversion and display. The setup corresponds approximately with curve (a) in Fig. 6.

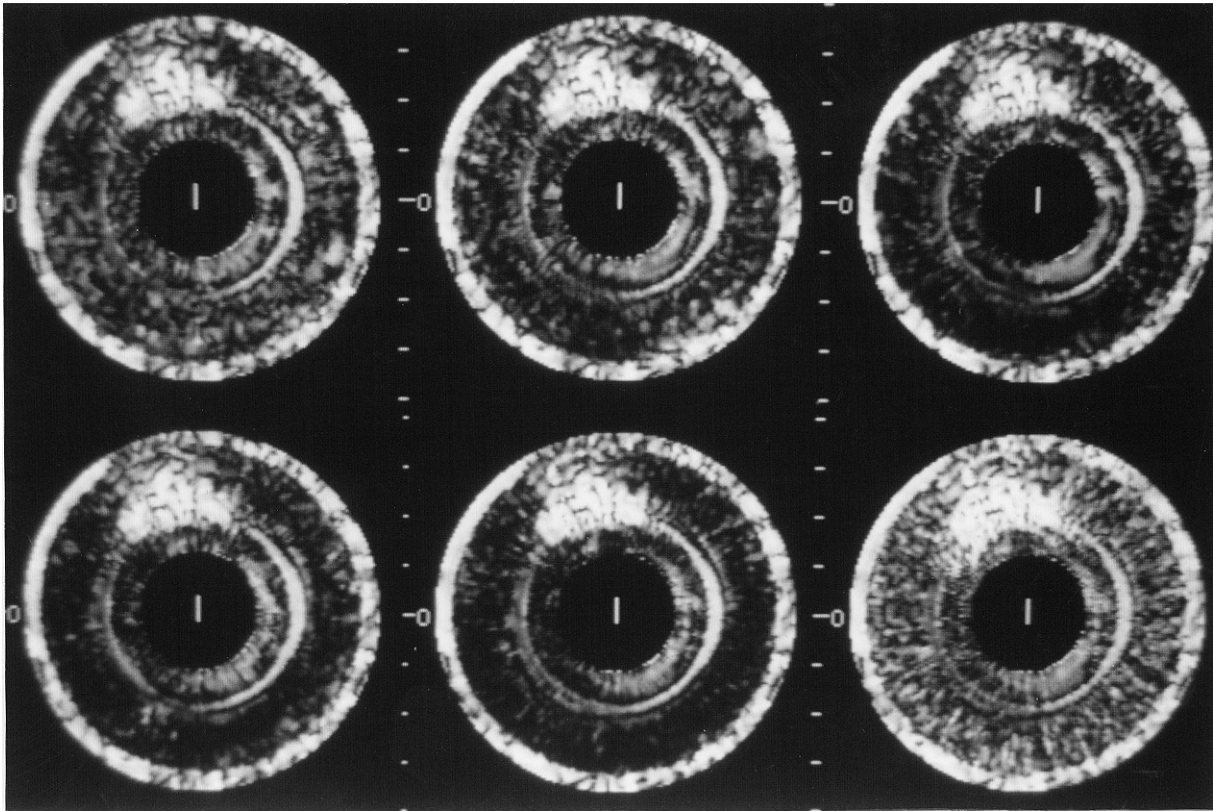


Fig. 7. Blood noise reduction by beam tilting and lateral low pass filtering with a filter of length 5. Water with blood mimicking particles immersed was flushed through a rubber hose of diameter 5 mm (the bright outer ring) and imaged with a 20 MHz (8 F) rotating mirror catheter: (a)  $V_B = 0 \text{ cm s}^{-1}$ , (b)  $V_B = 20 \text{ cm s}^{-1}$ , (c)  $V_B = 40 \text{ cm s}^{-1}$ , (d)  $V_B = 50 \text{ cm s}^{-1}$ , (e)  $V_B = 80 \text{ cm s}^{-1}$ , (f) A reference image with  $V_B = 0 \text{ cm s}^{-1}$  and no filter applied. Catheter artifacts are shown as a bright cloud between 11 and 12 o'clock and as rings close to the catheter.

## B. Results

A simple moving averaging filter was implemented in each depth location of the image, i.e. each of the 64 circular data segments consisting of 1024 lateral samples was filtered with a FIR-filter with rectangular impulse response. The filter order was increased until the desired vessel wall signal was slightly distorted (filter length = 5) to ensure that the cutoff frequency was set as low as possible for maximum blood noise reduction. The result of the test is shown in Fig. 7 for five different flushing velocities, from zero velocity in (a) and up to  $80 \text{ cm s}^{-1}$ , in (e). A significant blood noise reduction is obtained in (d) and (e) and where the velocity exceeds  $40 \text{ cm s}^{-1}$ , and this corresponds well with the simulation. The picture in (f) is a reference image with zero water velocity and *no filtering*. This image is more noisy than the image in (a) although both represent zero velocity. The reason is that the filter reduces not only blood noise, but also some electronic background noise present in all images. The display unit accepts 256 beams per frame which means that the filtered data is decimated from 1024 to 256 beams per revolution.

## IV. DISCUSSION AND CONCLUSION

Both the simulation and the *in vitro* experiment demonstrates that the lateral low pass filter reduces blood noise significantly for blood velocities exceeding  $50 \text{ cm s}^{-1}$  in a

typical 20 MHz imaging situation (8 F catheter with  $10^\circ$  tilt angle and frame rate equal to 15 f.p.s.). In an *in vivo* situation, this filter will reduce blood noise only in systole of peripheral arteries and rarely in coronary arteries.

The frequency separation and the filter efficiency can be increased by changing the ultrasound frequency, the beam tilt angle, the frame rate and the beam width (transducer aperture). The simulation shows that the blood noise reduction ratio improves dramatically by increasing the frequency to 30 or 40 MHz, increase the beam tilt angle to  $15^\circ$  and reduce the frame rate to 10 f.p.s. Unfortunately, the backscattered intensity from blood also increases with the ultrasound frequency, resulting in less contrast between blood and the vessel wall for very low blood velocities (when the filter is not effective), but better contrast for high blood velocities (when the filter is effective). Running the system with frame rates below 10 f.p.s. may be acceptable in vessels with little dilatation and/or catheter tip movements.

The blood velocity will vary with time and by image coordinates. The proposed model is able to predict the blood noise rejection ratio for a small sector (determined by the filter length) in a constant depth and for a known constant blood velocity in this area. The degree of blood noise reduction is therefor subject to variations across the lumen.

The experiment in Section III was carried out by applying a simple averaging filtering of length 5 to each depth location,

i.e. every lateral sample along the circle was the average of the 5 nearest neighbors. The filter bandwidth was the same for all depths. This is the correct choice as long as the beam width is proportional to range (as assumed in the model). However, using a focused beam means that the sample volume is broader outside the focus than the model predicts. For optimal performance one can implement filters that fit to the actual beam width in that particular depth. The price paid is increased cost and complexity.

The measurements includes an analog logarithmic amplifier while the simulations is based on a linear model. For this reason, the two methods cannot be compared directly. The log-amp causes the lateral spectrum from vessel wall and blood noise to be slightly broader than in the linear case, but a minor effect on the frequency separation is expected [16].

The low scattering from soft plaque makes discrimination between blood and plaque difficult. The proposed filter requires quite high velocities in order to reduce noise. This means that in situations where the catheter inhibits the blood flow (close to a tight lesion), little or no effect is obtained. Actually, soft plaque may be better visualized without an active blood noise filter in a real time situation due to the absence of fluctuating blood noise. The difference in temporal properties between blood noise (fluctuating) and vessel wall and soft plaque (stationary) may be used for automatic differentiation. Signal analysis along the temporal coordinate (frame to frame) is the topic for another paper that is in progress.

#### APPENDIX

The power spectrum in the lateral direction from stationary scatterers is modeled by (10). The following equations describe how this result is obtained, starting with (3) (leaving out  $\alpha$ ):

$$\begin{aligned} g(r, \phi, \psi) \\ = \alpha \int dr' d\phi' d\psi' h(r - r', \phi - \phi', \psi - \psi') \sigma(r', \phi', \psi'). \end{aligned} \quad (\text{A.1})$$

The Fourier transform of this equation is written

$$G(k_r, k_\phi, k_\psi) = H(k_r, k_\phi, k_\psi) \Sigma(k_r, k_\phi, k_\psi). \quad (\text{A.2})$$

The corresponding autocorrelation function of the received signal is given by

$$R_{3D}(r, \phi, \psi) = E\{g(r_0 + r, \phi_0 + \phi, \psi_0 + \psi)g(r_0, \phi_0, \psi_0)\}. \quad (\text{A.3})$$

If the scattering distribution is a stationary random process, the Wiener-Khintchine theorem can be applied to (A.2) yielding

$$P_{g3D}(k_r, k_\phi, k_\psi) = |H(k_r, k_\phi, k_\psi)|^2 P_\Sigma(k_r, k_\phi, k_\psi) \quad (\text{A.4})$$

where “ $P_{g3D}(k_r, k_\phi, k_\psi)$ ” is the power spectral density of  $g(r, \phi, \psi)$  in three dimensions.

A random stationary scattering distribution is characterized by the following autocorrelation function:

$$R_\sigma(r, \phi, \psi) = \delta(r)\delta(\phi)\delta(\psi) \quad (\text{A.5})$$

if the power spectrum is constant as assumed here:

$$P_\Sigma(k_r, k_\phi, k_\psi) = P_\Sigma \quad (\text{A.6})$$

The three-dimensional representation of the signal can be reduced to a two-dimensional (radial and lateral) representation by setting the azimuthal angle equal to zero in the autocorrelation function, i.e. integrating over the azimuthal frequency range:

$$R_{2D}(r, \phi) = R_{3D}(r, \phi, \psi = 0) \quad (\text{A.7})$$

The power spectrum in the lateral direction is then (for a constant range to the scatterers)

$$P_{g2D}(r, k_\phi) = \frac{1}{2\pi} \int dk_\psi P_{g3D}(k_r, k_\phi, k_\psi). \quad (\text{A.8})$$

Inserting (A.4) and (A.6) in (A.8) one obtains

$$\begin{aligned} P_{g2D}(r, k_\phi) &= \frac{1}{2\pi} \int dk_\psi |R_{FT}(k_r)|^2 \\ &\times |A_{FT}(k_\phi, k_\psi)|^2 P_\Sigma \end{aligned} \quad (\text{A.9})$$

where the Fourier transform of the impulse response  $H(k_r, k_\phi, k_\psi)$  is separated in a radial  $R_{FT}(k_r)$  and an angular term  $A_{FT}(k_\phi, k_\psi)$ . For a constant range “ $r$ ”, this yields the following expression for the one-dimensional power spectrum in the lateral direction for stationary scatterers:

$$P_{g\phi}(k_\phi) \sim \int dk_\psi |A_{FT}(k_\phi, k_\psi)|^2 \quad (\text{A.10})$$

This lateral spectrum is obtained by keeping the range parameter constant. In real imaging, scatterers from all depth locations within the sample volume will contribute to the signal. However, the spectra from different depths will all have the same shape as given by Eq. A.10. This model is therefore a good description of the lateral power spectrum from stationary scatterers.

#### ACKNOWLEDGMENT

A special thanks to Cardiovascular Imaging Systems Inc. for the support of components and equipment required to perform this work, and thanks to Atle Kleven for valuable comments on the English language.

#### REFERENCES

- [1] C. T. Lancee, N. Bom, and H. H. Rijndorp, Eds., *Construction of a Circular Ultrasonic Array with Miniature Elements for Cardiac Application* (Ultrasonics in Medicine), E. Kazner *et al.* Eds. Munich, Germany: Excerpta Medica: 1975.
- [2] N. Bom *et al.*, “Early and recent intraluminal ultrasound devices,” *Int. J. Cardiac Imaging*, vol. 4, pp. 79–88, 1989.
- [3] P. G. Yock, D. T. Linker, and B. A. J. Angelsen, “Two-dimensional intravascular ultrasound: Technical development and initial clinical experience,” *J. Am. Soc. Echocardiograph*, vol. 2, no. 4, pp. 296–304, 1989.
- [4] R. J. Crowley *et al.*, “Optimized ultrasound imaging catheters for use in the vascular system,” *Int. J. Cardiac Imaging*, vol. 4, pp. 145–151, 1989.
- [5] R. J. Crowley *et al.*, “Ultrasound guided therapeutic catheters: recent developments and clinical results,” *Int. J. Cardiac Imaging*, vol. 6, pp. 145–156, 1991.
- [6] R. W. Martin and C. C. Johnson, “Design characteristics for intravascular ultrasonic catheters,” *Int. J. Cardiac Imaging*, vol. 4, pp. 201–216, 1989.

- [7] N. Bom and J. R. T. C. Roelandt, "Intravascular ultrasound: Newest branch on the echo-tree," *Cardiovascular Imaging*, vol. 4, pp. 55–59, 1992.
- [8] G. Finet *et al.*, "Artifacts in intravascular ultrasound imaging: analyses and implications," *Ultrasound in Medicine and Biology*, vol. 19, pp. 533–547, 1993.
- [9] H. Hoff *et al.*, "Imaging artifacts in mechanically driven ultrasound catheters," *Int. J. Cardiac Imaging*, vol. 4, pp. 195–199, 1989.
- [10] J. S. Chae *et al.*, "Potential limitations of intravascular ultrasound imaging," *J. ACC*, vol. 15, pp. 28A, 1990.
- [11] J. S. Chae *et al.*, "Geometric accuracy of intravascular ultrasound imaging," *J. Am. Soc. Echocardiography*, vol. 5, pp. 577–587, 1992.
- [12] P. J. Fitzgerald *et al.*, "Errors in intravascular ultrasound imaging interpretation and measurements due to limited dynamic range," *Circulation*, vol. 84, pp. 438, 1991.
- [13] K. K. Shung, R. A. Siegelmann, and J. M. Reid, "Scattering of ultrasound by blood," *IEEE Trans. Biomed. Eng.*, vol. BME-23, pp. 460–467, 1976.
- [14] G. R. Lockwood, L. K. Ryan, and F. S. Foster, "Measurement of the ultrasonic properties of vascular tissues and blood from 35–65 MHz," *Ultrasound in Med. and Biol.*, vol. 17, pp. 653–666, 1991.
- [15] R. A. Roberts and C. T. Mullis, *Digital Signal Processing*. Reading, MA: Addison-Wesley, 1987.
- [16] A. Gronningsaeter, "reduction of acoustic and electronic noise in intravascular ultrasound imaging," Dr. Ing. thesis, Norwegian Institute of Technology, Trondheim, Norway, 1992.
- [17] M. G. M. de Kroon *et al.*, "Angle-dependent backscatter from the arterial wall," *Ultrasound in Medicine and Biology*, vol. 17, pp. 121–126, 1991.
- [18] C. Di Mario *et al.*, "The angle of incidence of the ultrasonic beam: A critical factor for the image quality in intravascular ultrasonography," *Amer. Heart J.*, vol. 125, pp. 442–448, 1993.
- [19] W. W. Nichols and M. F. O'Rourke, *McDonald's Blood Flow in Arteries: Theoretic, Experimental, and Clinical Principles*. London: Arnold, 1990.
- [20] A. Fronek, *Noninvasive Diagnostics in Vascular Disease*. New York: McGraw Hill, 1989.
- [21] F. Kajija *et al.*, "Evaluation of human coronary blood flow with an 80 channel 20 MHz pulsed Doppler velocimeter and zero-cross and Fourier transform methods during cardiac surgery," *Circulation*, vol. 74 (suppl III), pp. III-53–60, 1986.
- [22] M. Yamagishi *et al.*, "Validity of catheter-tip Doppler technique in assessment of coronary flow velocity and application of spectrum analysis method," *The Amer. J. Cardiology*, vol. 67, pp. 758–762, 1991.
- [23] D. E. Hokanson, "A phase-locked echo tracking system for recording arterial diameter changes in vivo," *J. Appl. Physiology*, vol. 32, pp. 728–733, 1972.



**Aage Gronningsaeter** received the M.S. and Ph.D. degrees in electrical engineering from the Norwegian Institute of Technology, Trondheim, Norway, in 1985 and 1993 respectively.

In 1986 he worked with development at the at Division of Engineering Cybernetics, and at Department of Biomedical Engineering, University of Trondheim, Norway. During the period 1988–92 he held a scholarship from the Norwegian Institute of Technology, interrupted by a nine-months stay in 1989 at Cardiovascular Imaging Systems Inc., Sunnyvale, CA. He is currently at Department of Biomedical Engineering, University of Trondheim, holding a post doctoral stipend from the Norwegian Research Council. His research interest are in high frequency ultrasound imaging and RF-signal processing.



**Bjørn A. J. Angelsen** (M'79–SM'82) received the M.S. and Dr. Techn. degrees from the Norwegian Institute of Technology, Trondheim, Norway, in 1971 and 1977, respectively.

From 1971 to 1972 he worked on infrared detectors at the Norwegian Defence Research Establishment, Kjeller, Norway. From 1972 to 1975 he held a stipend at the Norwegian Institute of Technology and from 1975 until 1982 he was with the Division of Control Engineering, The Foundation of Scientific and Industrial Research (SINTEF), Norwegian Institute of Technology, Trondheim, Norway. From 1977 to 1978 he was on leave at the Department of Electrical Engineering, University of California, Berkeley, CA, and the Division of Biomedical Engineering, Stanford Research Institute, Menlo Park, CA. Since 1980 he has been an Adjunct Professor of Biocybernetics and since 1983 a Professor of Biomedical Engineering at the University of Trondheim. His research interests include noninvasive diagnosis with emphasis on ultrasonic diagnosis.



**Audun Gresli** received the M.S. degree in electrical engineering from the Norwegian Institute of Technology, Trondheim, Norway, in 1989.

He was with AUROTECH Electronics AS, Tydal, Norway, in 1990, and with Department of Biomedical Engineering, University of Trondheim, Norway in 1991. Currently he is working as a research engineer at AUROTECH Electronics AS. He manages the development of RF and microwave circuits. His research interests include RF and microwave technology and computer modeling.



**Hans G. Torp** (M'92) received the M.S. and Dr. Tech. degrees from the University of Trondheim, Norway, in 1978 and 1992, respectively.

From 1979 to 1983 he worked at the Division of Automatic Control, The Foundation of Scientific and Industrial Research (SINTEF) in Trondheim. Since 1983 he has been working at the Department of Biomedical Engineering, Faculty of Medicine, University of Trondheim. He is currently a Research Fellow, holding a stipend from the Norwegian Research Council. His research areas include stochastic

signal/image processing with applications in ultrasonic imaging, Doppler and color flow imaging.



**David T. Linker** received his medical degree in 1976 from Stanford University, and a master's degree in biomedical engineering from the University of Washington in 1982.

After completing fellowship training in both adult and pediatric Cardiology, he joined the faculty of the University of Trondheim, Norway, in Biomedical Engineering and Cardiology, where his research included computer analysis of digital echocardiographic data, and, in collaboration with Dr. Paul Yock, the development of one of the earliest intravascular ultrasound imaging devices. He was the Chief of Echocardiography at the Thoraxcenter, Academic Hospital, Rotterdam, in the Netherlands. Dr. Linker has just joined the faculty of the University of Washington as an Associate Professor of Internal Medicine in the Division of Cardiology. He was the founding organizer of the subgroup on intravascular ultrasound of the Working Group on Echocardiography of the European Society of Cardiology.